IEEE Access
Multidisciplinary | Rapid Review | Open Access Journal

Received June 18, 2020, accepted July 7, 2020, date of publication July 20, 2020, date of current version July 28, 2020.

Digital Object Identifier 10.1109/ACCESS.2020.3010031

A Novel Nonlinear Second Order Hyperbolic Partial Differential Equation-Based Image Restoration Algorithm With Directional Diffusion

SHUAIJIE LI[1] AND ZHANJIANG ZHI[2]
[1]School of Mathematics and Statistics, Henan University of Science and Technology, Luoyang, 471023, China
[2]School of Mathematics and Statistics, Henan University, Kaifeng 475001, China

Corresponding author: Shuaijie Li (lsjiesysu@163.com)

This work was supported in part by the National Nature Science Foundation of China under Grant 11802086, in part by the Key Projects of Institutions of Higher Learning in Henan Province under Grant 19A110014, in part by the Key Research and Promotion Projects in Henan Province under Grant 192102210263, and in part by the Research Star-up Funds of Henan University of Science and Technology under Grant 13480032.

ABSTRACT Recently, variational and partial differential equation (PDE)-based algorithms have become very important for image restoration. In this study, we propose a new second order hyperbolic PDE model based on directional diffusion for image restoration. This hyperbolic PDE restoration model can simply diffuse along the edge's tangential direction in the observed image, thereby removing noise while preserving the image edges and fine details, which avoids the staircase effect in the restored image. An effective numerical scheme is proposed for handling the computation of our approach using the finite difference method. Successful image restoration experiments demonstrated that the proposed second order hyperbolic PDE-based model obtains superior performance compared with other models at preserving edges and it avoids the staircase effect.

INDEX TERMS Hyperbolic partial differential equation, direction diffusion, image restoration.

I. INTRODUCTION

This Digital images are inevitably corrupted by noise during image acquisition, compression, transmission, and other processes, and thus image denoising is an important research area in image processing and computer vision [1], where the aim is to restore a noisy or blurred image while preserving the features of the original image.

PDE-based and variational algorithms have become very important tools for image restoration, where many algorithms have been developed and applied in computer vision applications. The two most influential algorithms are the anisotropic diffusion model (PM) proposed by Perona and Malik [2], and the total variation (TV)-based model proposed by Rudin *et al.* [3]. The PM model was designed with the explicit goal of achieving a good trade-off between noise removal and edge preservation. Since the pioneering study by Perona and Malik, many variance-based models have been proposed, including the anisotropic diffusion model proposed by Weickert [4], Weickert and Schnörr [5], structure tensor diffusion [6], the manifold diffusion method [7], adaptive anisotropic diffusion based on a structure tensor [8], anisotropic diffusion based on band pass signals [9], a modified PM model based on directional Laplacian [10], and automatic parameter selection anisotropic diffusion [11]. The TV model has been studied extensively, thereby demonstrating that it is efficient for removing noise and preserving edges [12], [13]. Many improved models and optimization methods have also been proposed and applied, such as adaptive TV denoising [13], [14], the anisotropic higher degree TV regularizer [15], fixed point iteration [16], [17], primal-dual methods [18], [19], and split Bregman method [20]–[23].

However, nonlinear anisotropic partial differential equations (PDEs) and TV-based denoising often cause staircase effects [24]. Thus, to alleviate these staircase effects, high

The associate editor coordinating the review of this manuscript and approving it for publication was Byung Cheol Song.

order PDEs have been considered in recent years [25]–[28], such as the LLT (Lysaker M., Lundervold A., Tai X.C.) model [25], YK (You Y., Kaveh M.) model [26], and the adaptive fourth-order model [28], but high order PDEs inevitably corrupt the high-frequency details in the restored images, i.e., high order PDEs will over-smooth the images and affect the preservation of weak edges.

Recently, Barbu transformed the parabolic second-order and fourth-order PDEs into more effective hyperbolic diffusion models, and proposed second-order hyperbolic PDE (SOHPDE) [29] and fourth-order hyperbolic PDE (FOHPDE) [30] models for image restoration, which help to avoid the staircase effect as well as preserving the edges and features. Inspired by these new methods and the direction diffusion [31], in this study, we propose a new second-order nonlinear hyperbolic PDE model based on spatial directional diffusion (HPDEDD) for image restoration. Compared with other models, the proposed HPDEDD model has three advantages. First, the proposed HPDEDD model considers the structure of the observed image, where diffusion only occurs along the edges to preserve fine features. Second, hyperbolic diffusion helps to avoid the staircase effect. Third, the added edge detector facilitates selective smoothing to avoid blurred edges. Experimental comparisons with other PDE-based methods demonstrated that the proposed HPDEDD algorithm performs more effectively at high level noisy image restoration while also preserving the edges and avoiding the staircase effect.

The remainder of this paper is organized as follows. In Section 2, we define the directional diffusion operator. In Section 3, we propose the HPDEDD model and analyze the diffusion direction. We explain the efficient numerical implementation scheme for the proposed model in Section 4. In Section 5, we consider the selection of the parameters. In Section 6, we present the results of numerical experiments and comparisons with several existing methods in order to demonstrate the effectiveness of the HPDEDD model. Finally, we give our conclusions in the final section.

II. DIRECTIONAL DIFFUSION

The basic aim of image restoration is to recover an image $f(\mathbf{x})$ from an observed image $g(\mathbf{x})$. First, we present the definition of directional diffusion [10], [31]. Let us assume that an image region $\Omega \subset \mathbf{R}^2$, and $\mathbb{H}(\mathbf{x}) = \nabla^\top \nabla f(\mathbf{x})$ is a Hessian matrix of $f(\mathbf{x})$, where $\mathbf{x} = (x, y) \in \Omega$ and $\top$ denotes the transposition. $\vec{\mathbf{n}}\mathbb{H}(\mathbf{x})\vec{\mathbf{n}}^\top$ is the second order directional derivative of $f(\mathbf{x})$ along the direction $\vec{\mathbf{n}}$, where $\vec{\mathbf{n}}$ is a unit vector. Now, we define the directional diffusion $\Phi(\nabla f(\mathbf{x}))$:

$$\Phi(\nabla f(\mathbf{x})) = \vec{\mathbf{n}}\mathbb{H}(\mathbf{x})\vec{\mathbf{n}}^\top = \vec{\mathbf{n}}\nabla^\top \nabla f(\mathbf{x})\vec{\mathbf{n}}^\top. \tag{1}$$

We incorporate an edge detector $\Gamma(|\nabla_{G_\sigma} g|)$ for the observed image $g(\mathbf{x})$ into Eq. (1) in the following manner:

$$\Phi(\nabla f(\mathbf{x})) = \vec{\mathbf{n}}\nabla^\top(\Gamma(|\nabla_{G_\sigma} g|)\nabla f(\mathbf{x}))\vec{\mathbf{n}}^\top, \tag{2}$$

where

$$\Gamma(|\nabla_{G_\sigma} g|) = 1/(1 + |\nabla_{G_\sigma} g|),$$

$$|\nabla_{G_\sigma} g| = k_1|\nabla G_\sigma * g|^2 + k_2|\nabla^2 G_\sigma * g|^2, \tag{3}$$

k_1 and k_2 are positive constants, and G_σ is a Gaussian kernel with the standard deviation σ. In the edge detector, the term $|\nabla^2 G_\sigma * g|^2$ is added so the edge detector is better at identifying the weak edges or textures. $|\nabla^2 G_\sigma * g|^2$ is larger in the regions corresponding to the high frequency components than the low frequency components (smooth regions), so the proposed detector can identify strong edges or textures as well as weak edges or textures. Near the edges and textures where $|\nabla_{G_\sigma} g|$ is large, $\Gamma(|\nabla_{G_\sigma} g|)$ is close to zero, and thus the diffusion is weak. In the smooth regions $|\nabla_{G_\sigma} g|$ is small, so $\Gamma(|\nabla_{G_\sigma} g|)$ is close to one and the diffusion is strong. Thus, the proposed model can smooth selectively during image restoration. In summary, the edge detector improves the performance of the proposed model at preserving the edges and textures.

III. PROPOSED HPDEDD MODEL

1) HPDEDD RESTORATION MODEL

In the section, we present a nonlinear second-order PDE-based image restoration model based on the second-order hyperbolic diffusion equation, which is called the HPDEDD model, for effectively restoring noisy images while avoiding the staircase effect as well as preserving the edges and fine details. Using the directional diffusion operator defined in the previous section, the novel proposed HPDEDD model is the following second-order nonlinear hyperbolic initial boundary problem:

$$\alpha\frac{\partial^2 f}{\partial t^2} + \beta\frac{\partial f}{\partial t} - \Phi(\nabla f(\mathbf{x})) + \lambda(f(\mathbf{x}) - g(\mathbf{x})) = 0, \quad \mathbf{x} \in \Omega, t > 0, \tag{4}$$

with the initial condition:

$$\begin{cases} f(0, \mathbf{x}) = g(\mathbf{x}), & \mathbf{x} \in \Omega, \\ \frac{\partial f}{\partial t}(0, \mathbf{x}) = 0, & \mathbf{x} \in \Omega, \end{cases} \tag{5}$$

and the boundary conditions:

$$\frac{\partial f}{\partial \vec{N}}(t, \mathbf{x}) = 0, \quad \mathbf{x} \in \partial\Omega, \tag{6}$$

where $\Phi(\nabla f(\mathbf{x}))$ is defined in Eq. (2), the parameters α, β, λ are positive constants, and $\vec{N}$ is the normal direction on $\partial\Omega$.

2) ANALYSIS OF THE DIFFUSION DIRECTION $\vec{\mathbf{n}}$

The directional diffusion operator $\Phi(\nabla f(\mathbf{x}))$ in direction $\vec{\mathbf{n}}$ can be rewritten as:

$$\begin{aligned} &\Phi(\nabla f(\mathbf{x})) \\ &= \Gamma(|\nabla_{G_\sigma} g|)\vec{\mathbf{n}}\nabla^\top \nabla f(\mathbf{x})\vec{\mathbf{n}}^\top + \vec{\mathbf{n}}\nabla^\top \Gamma(|\nabla_{G_\sigma} g|)\nabla f(\mathbf{x})\vec{\mathbf{n}}^\top \\ &= \Gamma(|\nabla_{G_\sigma} g|)\vec{\mathbf{n}}\nabla^\top \nabla f(\mathbf{x})\vec{\mathbf{n}}^\top + (\nabla\Gamma(|\nabla_{G_\sigma} g|) \cdot \vec{\mathbf{n}}))(\nabla f(\mathbf{x}) \cdot \vec{\mathbf{n}}). \end{aligned} \tag{7}$$

The direction $\vec{\mathbf{n}}$ is very important for the diffusion operator and there are two influential directions, i.e., the edge's

gradient direction $\vec{\mathbf{n}}_1 = \frac{\nabla f}{|\nabla f|} = \frac{(f_x, f_y)}{|\nabla f|}$ and the edge's tangential direction $\vec{\mathbf{n}}_2 = \frac{(\nabla f)^\perp}{|\nabla f|} = \frac{(-f_y, f_x)}{|\nabla f|}$.

a) If $\vec{\mathbf{n}} = \vec{\mathbf{n}}_1 = \frac{\nabla f}{|\nabla f|}$, then $\Phi(\nabla f)$ should be:

$$\begin{aligned}&\Phi(\nabla f(\mathbf{x}))\\ &= \Gamma(|\nabla_{G_\sigma} g|)\vec{\mathbf{n}}\nabla^\top \nabla f(\mathbf{x})\vec{\mathbf{n}}^\top + (\nabla\Gamma(|\nabla_{G_\sigma} g|)\cdot\vec{\mathbf{n}}))(\nabla f(\mathbf{x})\cdot\vec{\mathbf{n}})\\ &= (\Gamma(|\nabla_{G_\sigma} g|) + |\nabla f(\mathbf{x})|\Gamma'(|\nabla_{G_\sigma} g|))f_{NN}, \qquad (8)\end{aligned}$$

where $f_{NN} = \frac{f_{xx}f_x^2 + f_{yy}f_y^2 + 2f_x f_y f_{xy}}{f_x^2 + f_y^2}$ is the second order derivative of the image $f(\mathbf{x})$ along the gradient direction. In this case, the PDE model (4) tends to diffuse along the gradient direction, which leads to blurring of the edges in the image $f(\mathbf{x})$.

b) If $\vec{\mathbf{n}} = \vec{\mathbf{n}}_2 = \frac{(\nabla f)^\perp}{|\nabla f|} = \frac{(-f_y, f_x)}{|\nabla f|}$, then $\Phi(\nabla f(\mathbf{x}))$ should be:

$$\begin{aligned}&\Phi(\nabla f(\mathbf{x}))\\ &= \Gamma(|\nabla_{G_\sigma} g|)\vec{\mathbf{n}}\nabla^\top \nabla f(\mathbf{x})\vec{\mathbf{n}}^\top + (\nabla\Gamma(|\nabla_{G_\sigma} g|)\cdot\vec{\mathbf{n}}))(\nabla f(\mathbf{x})\cdot\vec{\mathbf{n}})\\ &= \Gamma(|\nabla_{G_\sigma} g|)f_{TT}, \qquad (9)\end{aligned}$$

where $f_{TT} = \frac{f_{xx}f_y^2 + f_{yy}f_x^2 - 2f_x f_y f_{xy}}{f_x^2 + f_y^2}$ is the second order derivative of image $f(\mathbf{x})$ along the edge's tangential direction in the image $f(\mathbf{x})$. In this case, Eq. (4) tends to smooth along the edge's tangential direction to preserve the edges of the image $f(\mathbf{x})$. In fact, by diffusing along the edge's tangential direction in the image $f(x, y)$, it can preserve the edges but it may produce the staircase effect. Based on the analysis given above, it seems that choosing any of the aforementioned options for $\vec{\mathbf{n}}$ may not be adequate. Thus, in this study, we employ $\vec{\mathbf{n}} = \frac{(\nabla g)^\perp}{|\nabla g|} = \frac{(-g_y, g_x)}{|\nabla g|}$, so

$$\begin{aligned}&\Phi(\nabla f(\mathbf{x}))\\ &\quad= \vec{\mathbf{n}}\nabla^\top(\Gamma(|\nabla_{G_\sigma} g|)\nabla f(\mathbf{x}))\vec{\mathbf{n}}^\top\\ &\quad= \Gamma(|\nabla_{G_\sigma} g|)f_{gTT}(\mathbf{x}) + (\nabla\Gamma(|\nabla_{G_\sigma} g|)\cdot\vec{\mathbf{n}})(\nabla f(\mathbf{x})\cdot\vec{\mathbf{n}}), \qquad (10)\end{aligned}$$

where $f_{gTT} = \frac{f_{xx}g_y^2 + f_{yy}g_x^2 - 2g_x g_y f_{xy}}{g_x^2 + g_y^2}$ is the second order derivative of image $f(\mathbf{x})$ along the edge's tangential direction in the observed image $g(\mathbf{x})$. To alleviate the effect of noise when estimating $\vec{\mathbf{n}} = \frac{(\nabla g)^\perp}{|\nabla g|}$, the original image $g(\mathbf{x})$ is preprocessed with a Gaussian kernel with the standard deviation σ, i.e., $\nabla g = \nabla G_\sigma * g$. To further remove any noise, we add a smoothing term $\nu\Gamma(|\nabla_{G_\sigma} g|)\Delta f(\mathbf{x})$, so the directional diffusion $\Phi(\nabla f(\mathbf{x}))$ is finally written as:

$$\begin{aligned}\Phi(\nabla f(\mathbf{x})) = \vec{\mathbf{n}}\nabla^\top(\Gamma(|\nabla_{G_\sigma} g|)\nabla f(\mathbf{x}))\vec{\mathbf{n}}^\top\\ +\nu\Gamma(|\nabla_{G_\sigma} g|)\Delta f(\mathbf{x}), \qquad (11)\end{aligned}$$

where ν is a small constant.

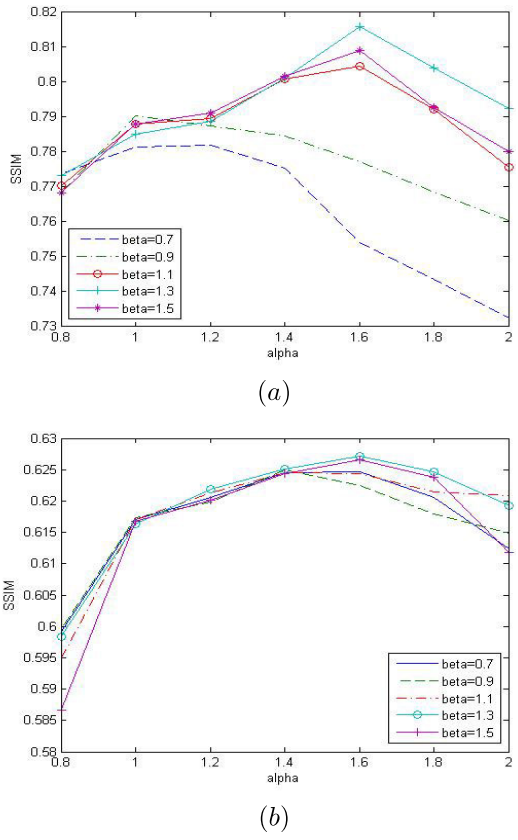

FIGURE 1. Effects of α and β on the image restoration results with noise variance: 30 and 100. Lena image: SSIM values for different α and β.

In summary, the proposed HPDEDD model considers the structure of the observed image and diffusion only occurs alone the edges to preserve fine features, while the hyperbolic diffusion helps to avoid the staircase effect, and the added edge detector facilitates selective smoothing to avoid blurred edges.

IV. NUMERICAL SCHEME

In this section, we explain the numerical implementation method for the proposed HPDEDD model (4–6) using a finite differences scheme. We perform the PDE discretization by considering a space grid with a size of h and a time step Δt. If the size of the original image is $M \times N$, then the space and time coordinates are quantized as:

$$\begin{aligned}x = ih, \quad y = jh, \quad \forall i \in \{0, 1, 2, \ldots, M\},\\ \forall j \in \{0, 1, 2, \ldots, N\}. \qquad (12)\end{aligned}$$

$$\begin{aligned}P_2 &= (\vec{\mathbf{n}}_x, \vec{\mathbf{n}}_y)\begin{pmatrix}((\Gamma(|\nabla_{G_\sigma} g|)f_x^n)_x & (\Gamma(|\nabla_{G_\sigma} g|)f_y^n)_x\\ (\Gamma(|\nabla_{G_\sigma} g|)f_x^n)_y & (\Gamma(|\nabla_{G_\sigma} g|)f_y^n)_y\end{pmatrix}\begin{pmatrix}\vec{\mathbf{n}}_x\\ \vec{\mathbf{n}}_y\end{pmatrix} + \nu\Gamma(|\nabla_{G_\sigma} g|)\Delta f^n\\ &= [(\Gamma(|\nabla_{G_\sigma} g|)f_x^n)_x\vec{\mathbf{n}}_x^2 + (\Gamma(|\nabla_{G_\sigma} g|)f_y^n)_y\vec{\mathbf{n}}_y^2] + [(\Gamma(|\nabla_{G_\sigma} g|)f_y^n)_x + (\Gamma(|\nabla_{G_\sigma} g|)f_x^n)_y]\vec{\mathbf{n}}_x\vec{\mathbf{n}}_y + \nu\Gamma(|\nabla_{G_\sigma} g|)\Delta f^n\\ &= [D_x^+(\Gamma(|\nabla_{G_\sigma} g|)D_x^- f^n)\vec{\mathbf{n}}_x^2 + D_y^+(\Gamma(|\nabla_{G_\sigma} g|)D_y^- f^n)\vec{\mathbf{n}}_y^2] + [D_x^+(\Gamma(|\nabla_{G_\sigma} g|)D_y^c f^n) + D_y^+(\Gamma(|\nabla_{G_\sigma} g|)D_x^c f^n)]\vec{\mathbf{n}}_x\vec{\mathbf{n}}_y\\ &\quad+\nu\Gamma(|\nabla_{G_\sigma} g|)\frac{f^n(i+h,j) + f^n(i-h,j) + f^n(i,j+h) + f^n(i,j-h) - 4f^n(i,j)}{h^2}, \qquad (14)\end{aligned}$$

FIGURE 2. Restoration results obtained using the different methods. The results in the second to fifth rows were obtained using the TV model [20], SOHPDE model [29], FOHPDE model [30], and the proposed model, respectively.

The approximations used in the finite differences scheme are explained as follows. Eq. (4) comprises three parts. The first part, $P_1 = \alpha \frac{\partial^2 f}{\partial t^2} + \beta \frac{\partial f}{\partial t}$, is approximated by using finite differences:

$$\begin{aligned} P_1 &= \alpha \frac{\partial^2 f}{\partial t^2} + \beta \frac{\partial f}{\partial t} \\ &= \alpha \frac{f^{n+\Delta t}(i,j) + f^{n-\Delta t}(i,j) - 2f^n(i,j)}{\Delta t^2} \\ &\quad + \beta \frac{f^{n+\Delta t}(i,j) + f^{n-\Delta t}(i,j)}{2\Delta t} \\ &= \frac{2\alpha + \beta \Delta t}{2\Delta t^2} f^{n+\Delta t}(i,j) + \frac{2\alpha - \beta \Delta t}{2\Delta t^2} f^{n-\Delta t}(i,j) \\ &\quad - \frac{2f^n(i,j)}{\Delta t^2}. \end{aligned} \tag{13}$$

The second part, $P_2 = \vec{\mathbf{n}} \nabla^\top (\Gamma(|\nabla_{G_\sigma} g|) \nabla f) \vec{\mathbf{n}}^\top + \nu \Gamma(|\nabla_{G_\sigma} g|) \Delta f$, can be rewritten as shown in Eq.(14), as shown at the bottom of the previous page, where

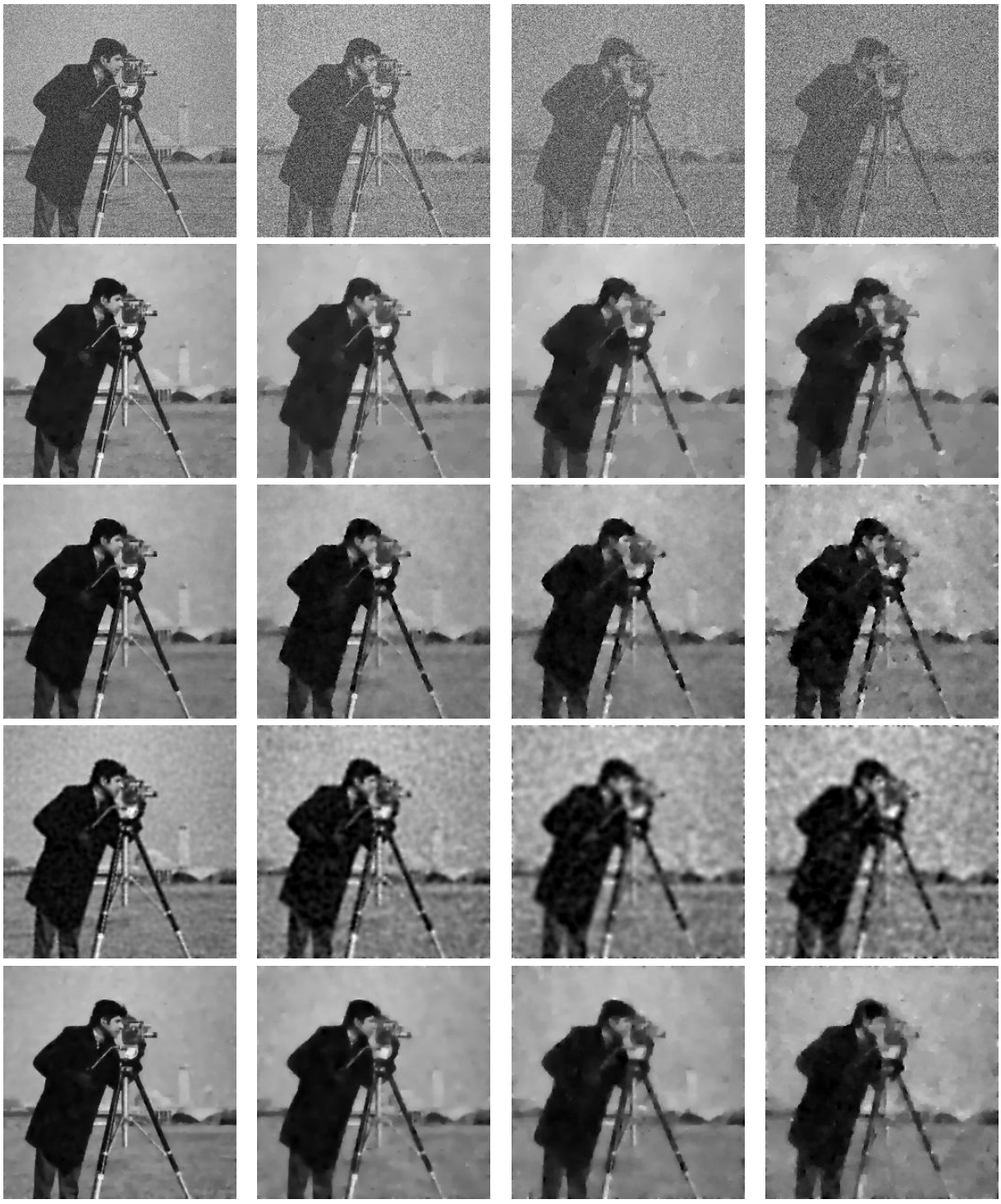

FIGURE 3. Restoration results obtained using the different methods. The results in the second to fifth rows were obtained using the TV model [20], SOHPDE model [29], FOHPDE model [30], and the proposed HPDEDD model, respectively.

$\vec{\mathbf{n}} = (\vec{\mathbf{n}}_x, \vec{\mathbf{n}}_y)$, $\vec{\mathbf{n}}_x = \frac{-g_y}{|\nabla g|}$, $\vec{\mathbf{n}}_y = \frac{g_x}{|\nabla g|}$, and these differential operator $D_x^{\pm}$, $D_y^{\pm}$, D_x^c, D_y^c are defined as

$$D_x^{\pm} s^n(i,j) = \pm \frac{s^n(i \pm h, j) - s^n(i,j)}{h},$$
$$D_y^{\pm} s^n(i,j) = \pm \frac{s^n(i, j \pm h) - s^n(i,j)}{h},$$

$$D_x^c s^n(i,j) = \frac{s^n(i+h, j) - s^n(i-h, j)}{2h},$$
$$D_y^c s^n(i,j) = \frac{s^n(i, j+h) - s^n(i, j-h)}{2h}.$$

Therefore, we can obtain the numerical approximation of the HPDEDD by $P1 - P2 + \lambda(f^n - g) = 0$. If we take $h = 1$ and $\Delta t = 1$, then we have the following explicit

FIGURE 4. Restoration results obtained using the different methods. The results in the second to fifth rows were obtained using the TV model [20], SOHPDE model [29], FOHPDE model [30], and the proposed HPDEDD model, respectively.

numerical implementation scheme for the hyperbolic PDE model:

$$f^{n+1}(i,j) = \frac{4}{2\alpha+\beta}f^{n}(i,j) - \frac{2\alpha-\beta}{2\alpha+\beta}f^{n-1}(i,j) + \frac{2}{2\alpha+\beta}P_2 - \frac{2\lambda}{2\alpha+\beta}(f^{n}(i,j) - g(i,j)). \quad (15)$$

The iterative algorithm begins with the original noisy image g and iterates until the steady state using Eq. (15) for $n = 1, 2, 3, \ldots$.

V. PARAMETER SELECTION

In this section, we explain the method for selecting the parameters used in our experiments. In the edge detector, k_1 and

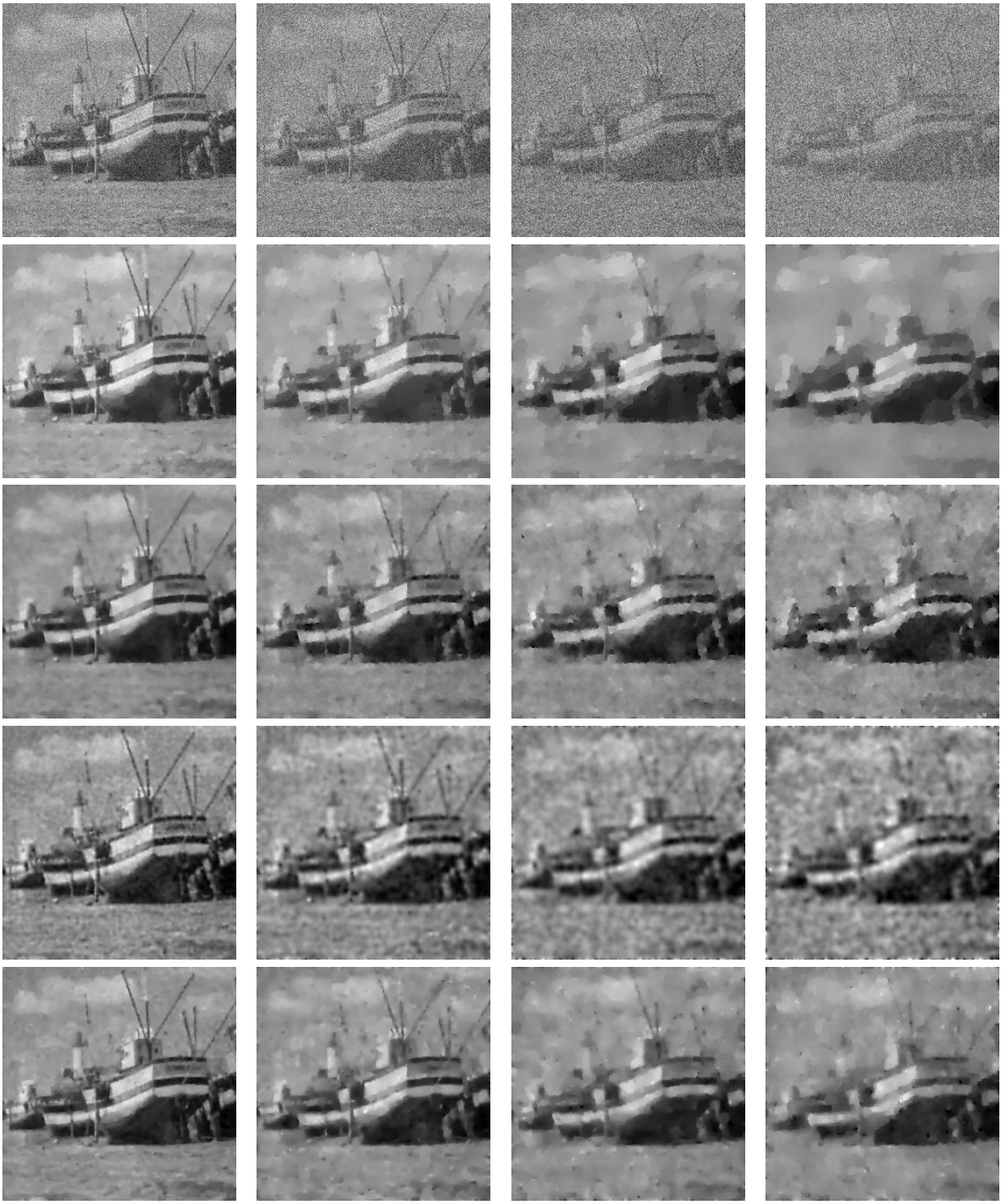

FIGURE 5. Restoration results obtained using the different methods. The results in the second to fifth rows were obtained using the TV model [20], SOHPDE model [29], FOHPDE model [30], and the proposed HPDEDD model, respectively.

k_2 are used to control the effect of the edge detector, and λ controls the fidelity term, but the denoising results would not adequate if they are excessively small or large. Based on many edge detection experiment, we found that $k_1 = 0.001$, $k_2 = 0.01$, and a Gaussian kernel G_σ with zero mean and variance $\sigma = 1.5$ were highly appropriate values. We also

TABLE 1. Quantitative analysis of the four methods with different noise levels.

Image	Noise	TV			SOHPDE			FOHPDE			HPDEDD		
		SNR	MSE	SSIM	SNR	MSE	SSIM	SNR	MSE	SSIM	SNR	MSE	SSIM
Lena	25	13.5914	99.3859	0.8154	12.8778	117.1349	0.7934	12.3982	130.8090	0.7717	13.6041	99.0959	0.8159
	50	10.8995	184.7628	0.7301	10.7977	189.0983	0.7247	9.9781	228.3763	0.6669	10.8964	184.1556	0.7337
	75	9.2054	272.8499	0.6726	9.2613	269.3577	0.6665	8.5025	320.7865	0.6102	9.2765	268.4205	0.6797
	100	8.3062	335.6193	0.6190	8.1517	347.7718	0.6005	7.4718	406.7060	0.5652	8.3526	328.7987	0.6284
Cameraman	25	15.1478	118.7875	0.8074	13.5900	170.0387	0.7794	12.5125	217.9218	0.7202	14.5840	135.2550	0.7944
	50	12.0280	243.6421	0.7330	11.7113	267.0736	0.7095	10.4308	351.9388	0.6047	11.6720	264.4532	0.7242
	75	10.4216	352.6866	0.6787	10.3864	355.5622	0.6606	8.9672	492.9775	0.5558	10.4335	350.8808	0.6796
	100	9.5666	429.4295	0.6496	9.4760	438.4828	0.5791	8.3065	573.9792	0.4898	9.5785	428.8861	0.6637
Pepper	25	15.2121	84.8347	0.8515	14.4966	100.0294	0.8458	13.4550	127.1418	0.8169	15.3155	82.8385	0.8505
	50	12.0187	176.9769	0.7743	11.8086	185.7502	0.7705	10.7647	236.2224	0.7283	11.9624	179.2864	0.7822
	75	10.2509	265.8860	0.7075	10.0397	279.1355	0.7159	9.4535	319.4734	0.6718	10.2649	265.4841	0.7237
	100	8.9177	361.4257	0.6682	8.9039	362.5714	0.6325	8.4166	405.6274	0.6132	8.9281	360.2268	0.6727
Boat	25	12.8620	103.0901	0.7838	11.9582	126.9379	0.7485	12.4579	113.1413	0.7641	12.9663	100.6434	0.7845
	50	9.8603	205.7707	0.6630	9.8879	204.4674	0.6686	9.5019	223.4738	0.6428	10.1492	192.5264	0.6778
	75	8.3318	292.5713	0.5956	8.5572	277.7753	0.6095	7.8695	325.4339	0.5736	8.4923	281.9579	0.6101
	100	7.2192	377.9982	0.5478	7.3753	364.6565	0.5504	6.8428	412.2194	0.5338	7.4381	359.4242	0.5620
Panda	25	16.6810	92.9724	0.7302	16.1542	104.9648	0.7152	15.8188	113.3908	0.7052	16.6179	94.3380	0.7272
	50	14.0595	170.0247	0.6328	14.2443	162.9394	0.6424	13.3688	199.3329	0.6178	14.2170	163.9668	0.6450
	75	12.6634	234.4860	0.5847	12.7656	229.0324	0.5892	12.0480	270.1805	0.5661	12.7841	228.0581	0.5971
	100	11.8898	280.2081	0.5552	11.6241	297.8875	0.5387	10.9166	350.5929	0.5172	11.8940	280.1787	0.5663

TABLE 2. Average values with different noise levels corresponding to the results in Table 1.

Noise	TV			SOHPDE			FOHPDE			HPDEDD		
	SNR	MSE	SSIM	SNR	MSE	SSIM	SNR	MSE	SSIM	SNR	MSE	SSIM
25	14.6988	99.8141	0.7977	13.8154	123.8211	0.7765	13.3285	140.4809	0.7556	14.6176	102.4342	0.7945
50	11.7732	196.2354	0.7066	11.6900	201.8658	0.7031	10.8089	247.8688	0.6521	11.7794	197.0258	0.7126
75	10.1746	283.6960	0.6478	10.2020	282.1726	0.6483	9.3681	345.7704	0.5955	10.2503	278.9603	0.6580
100	9.1799	356.9362	0.6080	9.1062	362.2740	0.5802	8.3909	429.8250	0.5438	9.2383	350.9028	0.6186

TABLE 3. Average values for each image with all noise levels corresponding to the results in Table 1.

Image	TV			SOHPDE			FOHPDE			HPDEDD		
	SNR	MSE	SSIM	SNR	MSE	SSIM	SNR	MSE	SSIM	SNR	MSE	SSIM
Lena	10.5006	223.1545	0.7093	10.2721	230.8407	0.6963	9.5877	271.6694	0.6535	10.5324	220.1177	0.7144
Cameraman	11.7910	286.1364	0.7172	11.2909	307.7893	0.6822	10.0543	409.2043	0.5926	11.5670	294.8688	0.7155
Pepper	11.5999	222.2808	0.7501	11.3122	231.8716	0.7412	10.5225	272.1163	0.7075	11.6177	221.9589	0.7573
Boat	9.5683	244.8576	0.6476	9.4447	243.4593	0.6442	9.1680	268.5671	0.6286	9.7615	233.6380	0.6586
Panda	13.8234	194.4228	0.6257	13.6970	198.7060	0.6214	13.0381	233.3743	0.6016	13.8783	191.6354	0.6339

fixed $\nu = 0.5, \lambda = 0.01$ because these settings obtained the best results based on many experimental proofs. There are two very important parameters in the hyperbolic PDE, i.e., α and β, which are the coefficients of the second order and first order derivatives in the time variable t. We tested different values of α, β to obtain the restored image with the highest structural similarity (SSIM) [32] value, and found that $\alpha \in [0.8, 2.0]$, $\beta \in [0.7, 1.5]$ were the best for image restoration. We experimentally determined the optimal parameters α, β in the following manner: α ranging from 0.8 to 2.0 and β ranging from 0.7 to 1.5 with a step size of 0.2 based on the Lena image, as shown in Fig. 1(a) (low level noise variance 30) and Fig. 1(b) (high level noise variance 100), where the noisy image was created by adding Gaussian noise using the Matlab function $Lena + randn(size(Lena)) \times variance$. Thus, we selected $\alpha = 1.6$, $\beta = 1.3$ for image restoration in the following experiments because they obtained the largest SSIM value.

VI. NUMERICAL EXPERIMENTS

We tested the efficiency and feasibility of the proposed model, and the results are presented in this section. We compared the restoration results obtained by the proposed HPDEDD model with those produced by the TV using split Bregman [20], SOHPDE [29], and FOHPDE [30] models. To objectively measure the image restoration quality, we employed the signal to noise ratio (SNR) in decibels (dB), mean squared error (MSE), and SSIM [32], which are defined as:

$$SNR = 10\log_{10}\frac{\|u-\bar{u}\|_2^2}{\|u-u^*\|_2^2}, \tag{16}$$

$$MSE = \frac{\|u-u^*\|_2^2}{|\Omega|}, \tag{17}$$

$$SSIM = \frac{(2\bar{u}\bar{u^*}+C_1)(2\sigma_{uu^*}+C_2)}{(\bar{u}^2+\bar{u^*}^2+C_1)(\sigma_u+\sigma_{u^*}+C_2)}, \tag{18}$$

where u^* and u are the inpainting image and true image, respectively; $\bar{u}$ and $\bar{u^*}$ are the mean values of u and u^*; σ_u and σ_{u^*} represent the variances of u and u^*; σ_{uu^*} is the covariance of u and u^*; and C_1 and C_2 are constants selected by considering the human visual system perception and to ensure the numerical stability of the division. The SNR, MSE, and SSIM have been used widely to test the quality of restored images, where the quality of the restored image is better when

FIGURE 6. Restoration results obtained using the different methods. The results in the second to fifth rows were obtained using the TV model [20], SOHPDE model [29], FOHPDE model [30], and the proposed HPDEDD model, respectively.

the values of SNR and SSIM are higher, and the value of MSE is lower.

In our experiments, the restoration results for TV using split Bregman [20] were obtained from the source code available from: http://dx.doi.org/10.5201/ipol.2012.g-tvi. The parameters for TV, SOHPDE, and FOHPDE were recommended in previous studies [20], [29], [30]. The parameters selected for the models were discussed in the previous section and they obtained the best results according to many experimental proofs. It should be noted that the stopping condition for each algorithm was that producing the best SSIM values.

First, we tested the denoising performance of the proposed method with five popular images at four different noise levels, where some of the noisy images tested are shown in the first rows of Figs. 2–5. The noisy images were created by adding Gaussian noise using the Matlab function $Image + randn(size(Image)) \times variance$, with variances of 25, 50, 75, and 100. The experimental results in terms of the SNR, MSE, and SSIM are shown in Table 1. According to Table 1, the proposed model obtained better values for SNR, MSE, and SSIM in most of the denoising results compared with the other models, especially the denoising results with high level noise (such as the SSIM values for Boat and Panda).

To further compare the performance of the different algorithms, we also present the corresponding average SNR, MSE, and SSIM values with four different noise levels in Table 2, and the corresponding average SNR, MSE, and SSIM values for each image in Table 3. Table 2 shows that the proposed model obtained the best average values for SNR, MSE, and SSIM, except with the low noise level (variance = 25), and the next best performance was with the TV model using the split-Bregman method, followed by the SOHPDE and FOHPDE models. For example, the proposed model obtained higher average SSIM values than the TV with split-Bregman method, SOHPDE model, and FOHPDE model, thereby demonstrating that the proposed model performed better than the other models under different noise levels. Table 3 shows that the proposed model obtained the highest average SNR, MSE, and SSIM values, except with the Cameraman image (because the values obtained using the proposed model were less than the values with the TV model for the Cameraman image when the noise level was low, e.g., variances of 25 and 50). Therefore, the proposed model is suitable for different types of images. Thus, we consider that the average image restoration performance of the proposed model is better than that of the other three models.

Second, we performed visual comparisons of the restored images. The denoising results obtained for the four noisy images with noise levels varying from 25 to 100 are shown in Figs. 2–6. According to the image restoration results in Figs. 2–6, the proposed model could remove various levels of noise while preserving the details and sharp edges, as well as avoiding the staircase effect. The TV model was affected severely by the staircase effect with high noise. The SOHPDE model was better at the preserving the edges and for avoiding the staircase effect than the TV model, but it performed worse when the noise level was very high. The FOHPDE model was not affected by the staircase effect, but it failed to remove the noise well and it blurred the sharp edges. Thus, the proposed model obtained better visual resolution than the other three models.

VII. CONCLUSION

In this study, we proposed a new second order hyperbolic PDE for image restoration based on directional diffusion in order to preserve the edges and fine details in images, as well as avoiding the staircase effect. The proposed PDE model can diffuse along the tangential direction of the edges in the observed image, thereby preserving the features in the image and the staircase effect never appears in the restored image. Numerous experiments using images with different noise levels demonstrated the effectiveness of the proposed second order hyperbolic PDE model. In particular, the experiments showed that the proposed model performed better than several existing methods, i.e., TV-based smoothing, the SOHPDE model, and the FOHPDE model.

REFERENCES

[1] P. Chatterjee and P. Milanfar, "Is denoising dead?" *IEEE Trans. Image Process.*, vol. 19, no. 4, pp. 895–911, Apr. 2010.
[2] P. Perona and J. Malik, "Scale-space and edge detection using anisotropic diffusion," *IEEE Trans. Pattern Anal. Mach. Intell.*, vol. 12, no. 7, pp. 629–639, Jul. 1990.
[3] L. I. Rudin, S. Osher, and E. Fatemi, "Nonlinear total variation based noise removal algorithms," *Phys. D, Nonlinear Phenomena*, vol. 60, nos. 1–4, pp. 259–268, Nov. 1992.
[4] J. Weickert, *Anisotropic Diffusion in Image Processing*. Stuttgart, Germany: Taeubner, 1998.
[5] J. Weickert and C. Schnörr, "PDE-based preprocessing of medical images," *Künstliche Intell.*, vol. 2000, no. 3, pp. 5–10, 2000.
[6] J. Weickert, "Coherence-enhancing diffusion filtering," *Int. J. Comput. Vis.*, vol. 31, nos. 2–3, pp. 111–127, 1999.
[7] N. Sochen, R. Kimmel, and R. Malladi, "A general framework for low level vision," *IEEE Trans. Image Process.*, vol. 7, no. 3, pp. 310–318, Mar. 1998.
[8] K. Liu, J. Tan, and B. Su, "Adaptive anisotropic diffusion for image denoising based on structure tensor," in *Proc. 5th Int. Conf. Digit. Home*, Nov. 2014, pp. 111–116.
[9] S. Mahmoodi, "Anisotropic diffusion for noise removal of band pass signals," *Signal Process.*, vol. 91, no. 5, pp. 1298–1307, May 2011.
[10] Y. Q. Wang, J. Guo, W. Chen, and W. Zhang, "Image denoising using modified Perona–Malik model based on directional Laplacian," *Signal Process.*, vol. 93, no. 9, pp. 2548–2558, Sep. 2013.
[11] M. Heydari, M.-R. Karami, and A. Babakhani, "A new adaptive coupled diffusion PDE for MRI Rician noise," *Signal, Image Video Process.*, vol. 10, no. 7, pp. 1211–1218, Oct. 2016.
[12] Y. Chen and M. Rao, "Minimization problems and associated flows related to weighted p energy and total variation," *SIAM J. Math. Anal.*, vol. 34, no. 5, pp. 1084–1104, Jan. 2003.
[13] Y. Chen and T. Wunderli, "Adaptive total variation for image restoration in BV space," *J. Math. Anal. Appl.*, vol. 272, no. 1, pp. 117–137, Aug. 2002.
[14] Q. Chen, P. Montesinos, Q. S. Sun, P. A. Heng, and D. S. Xia, "Adaptive total variation denoising based on difference curvature," *Image Vis. Comput.*, vol. 28, no. 3, pp. 298–306, Mar. 2010.
[15] Y. Hu and M. Jacob, "Higher degree total variation (HDTV) regularization for image recovery," *IEEE Trans. Image Process.*, vol. 21, no. 5, pp. 2559–2571, May 2012.
[16] T. F. Chan and P. Mulet, "On the convergence of the lagged diffusivity fixed point method in total variation image restoration," *SIAM J. Numer. Anal.*, vol. 36, no. 2, pp. 354–367, Jan. 1999.
[17] A. Chambolle and P.-L. Lions, "Image recovery via total variation minimization and related problems," *Numerische Math.*, vol. 76, no. 2, pp. 167–188, Apr. 1997.
[18] M. Nikolova, "An algorithm for total variation minimization and applications," *J. Math. Imag. Vis.*, vol. 20, no. 1/2, pp. 89–97, Jan. 2004.
[19] T. F. Chan, G. H. Golub, and P. Mulet, "A nonlinear primal-dual method for total variation-based image restoration," *SIAM J. Sci. Comput.*, vol. 20, no. 6, pp. 1964–1977, Jan. 1999.
[20] P. Getreuer, "Rudin-Osher-Fatemi total variation denoising using split Bregman," *Image Process. Line*, vol. 2, pp. 74–95, May 2012.
[21] X. Liu and L. Huang, "Split Bregman iteration algorithm for total bounded variation regularization based image deblurring," *J. Math. Anal. Appl.*, vol. 372, no. 2, pp. 486–495, Dec. 2010.
[22] T. Goldstein and S. Osher, "The split Bregman method for L1-regularized problems," *SIAM J. Imag. Sci.*, vol. 2, no. 2, pp. 323–343, Jan. 2009.

[23] X. Liu and L. Huang, "Total bounded variation-based Poissonian images recovery by split Bregman iteration," *Math. Methods Appl. Sci.*, vol. 35, no. 5, pp. 520–529, Mar. 2012.
[24] M. Nikolova, "Weakly constrained minimization: Application to the estimation of images and signals involving constant regions," *J. Math. Imag. Vis.*, vol. 21, no. 2, pp. 155–175, Sep. 2004.
[25] M. Lysaker, A. Lundervold, and X.-C. Tai, "Noise removal using fourth-order partial differential equation with applications to medical magnetic resonance images in space and time," *IEEE Trans. Image Process.*, vol. 12, no. 12, pp. 1579–1590, Dec. 2003.
[26] Y.-L. You and M. Kaveh, "Fourth-order partial differential equations for noise removal," *IEEE Trans. Image Process.*, vol. 9, no. 10, pp. 1723–1730, Oct. 2000.
[27] M. R. Hajiaboli, "An anisotropic fourth-order diffusion filter for image noise removal," *Int. J. Comput. Vis.*, vol. 92, no. 2, pp. 177–191, Apr. 2011.
[28] S. Li and X. Yang, "Novel image inpainting algorithm based on adaptive fourth-order partial differential equation," *IET Image Process.*, vol. 11, no. 10, pp. 870–879, Oct. 2017.
[29] T. Barbu, "Nonlinear PDE model for image restoration using second-order hyperbolic equations," *Numer. Funct. Anal. Optim.*, vol. 36, no. 11, pp. 1375–1387, Nov. 2015.
[30] T. Barbu, "Nonlinear fourth-order hyperbolic PDE-based image restoration scheme," in *Proc. 5th IEEE Int. Conf. E-Health Bioeng. (EHB)*, Nov. 2015, pp. 1–4.
[31] S. Li, "Second-order PDE-based image restoration algorithm using directional diffusion," *J. Eng.*, vol. 2017, no. 7, pp. 327–332, Jul. 2017.
[32] Z. Wang, A. C. Bovik, H. R. Sheikh, and E. P. Simoncelli, "Image quality assessment: From error visibility to structural similarity," *IEEE Trans. Image Process.*, vol. 13, no. 4, pp. 600–612, Apr. 2004.

SHUAIJIE LI received the B.S. degree in mathematics from Anyang Normal University, Anyang, China, in 2005, the M.S. degree in applied mathematics from Henan University, Kaifeng, China, in 2008, and the Ph.D. degree in applied mathematics from Sun Yat-sen University, Guangzhou, China, in 2012.

From 2012 to 2020, he was a Lecturer with the School of Mathematics and Statistics, Henan University of Science and Technology. From 2016 to 2017, he was a Visiting Scholar with the Department of Mathematics, University of Florida, Gainesville, FL, USA. He is the author of 16 articles and two inventions. His research interests include partial differential equations, numerical computation, and image processing.

ZHANJIANG ZHI received the B.S. degree in mathematics and the M.S. degree in applied mathematics from Henan University, Kaifeng, China, in 2003 and 2008, respectively, and the Ph.D. degree in signal and information processing from the Dalian University of Technology, Dalian, China, in 2016.

From 2003 to 2020, he was a Lecturer. From 2019 to 2020, he was an Assistant Professor with the School of Mathematics, Henan University. His research interests include image processing and machine learning.